Arch. Metall. Mater. **71** (2026), 2, 605-609

DOI: https://doi.org/10.24425/amm.2026.158851

DONG HOON LEE[1], KYUNG-SHIK YOON[1], HEE YEON JEON[1], JEONG HYUN KIM[1], JUNG-YEUL YUN[2], SUNG-TAG OH[1], YOUNG-IN LEE[1*]

ENHANCING FILTRATION PERFORMANCE OF SINTERED METAL FILTERS THROUGH PORE STRUCTURE MODIFICATION USING FINE FLAKE-SHAPED PARTICLES

Sintered metal gas filters commonly suffer from a trade-off between filtration efficiency and gas permeability due to limited control over pore structure. In this study, fine flake-shaped stainless steel 316L powders were introduced into a sintered filter matrix to modify pore geometry without significantly reducing porosity. Microstructural and pore analyses showed that flake addition subdivided interparticle voids, leading to reduced pore size while maintaining high open porosity at low flake contents. Notably, the filter containing 1 wt.% flake-shaped powder exhibited a clear improvement in filtration efficiency without a pronounced increase in pressure drop. At higher flake contents, further gains in filtration efficiency were accompanied by a rapid increase in flow resistance. This work demonstrates that the controlled incorporation of fine flake-shaped powders provides a simple and scalable approach to pore-structure engineering for high-performance metal gas filters.

Keywords: Sintered metal filter; Pore structure engineering; Flake-shaped powder; Gas filtration

1. Introduction

As semiconductor manufacturing advances toward increasingly miniaturized and complex device architectures, particulate contamination generated during processing has become a critical concern affecting device yield and reliability [1,2]. Consequently, the effective removal of fine impurities and the stable supply of ultra-high-purity gases are essential requirements in modern semiconductor fabrication. In processes such as epitaxy, deposition, ion implantation, etching, and sputtering, a wide range of process gases are employed, including corrosive species such as HCl, BCl_3, and CF_4 [3,4]. These gases can induce severe corrosion of reaction chambers, pipelines, and filtration components, necessitating gas filters that combine high corrosion resistance with reliable microfiltration performance.

Porous metal filters have attracted significant attention for semiconductor gas filtration due to their superior mechanical strength, thermal stability, and chemical durability compared with polymeric and ceramic filters [5,6,13]. Among various fabrication routes, powder metallurgy-based sintered metal filters are widely adopted because of their simplicity, scalability, and cost-effectiveness [7,8]. In this approach, pore size and porosity are primarily controlled through the selection of powder size and size distribution, as well as compaction and sintering conditions. However, conventional sintered filters typically rely on large irregular powders, which tend to form relatively simple pore networks [8,9]. As a result, attempts to improve filtration efficiency by reducing pore size often lead to a substantial loss of porosity and gas permeability, giving rise to an inherent trade-off between particle removal efficiency and pressure drop.

Recent studies have suggested that filtration performance is not governed solely by pore size, but also by pore geometry and flow path complexity [10-12]. Increasing the complexity of gas flow paths can enhance particle capture mechanisms such as inertial impaction, diffusion, and interception, without necessarily relying on excessive densification. Nevertheless, achieving such complex pore architectures within the conventional powder metallurgy framework remains challenging, as simple packing of spherical particles provides limited freedom to tailor pore geometry independently from porosity.

In this context, the incorporation of fine flake-shaped particles can offer a promising strategy for engineering pore structures in sintered metal filters. Owing to their high aspect ratio and large specific surface area, flake-shaped particles can

[1] SEOUL NATIONAL UNIVERSITY OF SCIENCE AND TECHNOLOGY, DEPARTMENT OF MATERIALS SCIENCE AND ENGINEERING, SEOUL 01811, REPUBLIC OF KOREA
[2] NANO MATERIALS RESEARCH DIVISION, KOREA INSTITUTE OF MATERIALS SCIENCE, CHANGWON 51508, REPUBLIC OF KOREA

* Corresponding author: youngin@seoultech.ac.kr

partially occupy interparticle voids and disrupt straight flow channels when incorporated into a powder matrix. This geometric effect is expected to reduce the effective pore size and increase flow path complexity while maintaining a high overall porosity. Importantly, the extent of these structural modifications can be strongly influenced by the flake particle content, implying that pore structure and filtration behavior can be tuned through controlled addition rather than uniform pore shrinkage.

Based on this concept, this study investigates the effect of fine flake-shaped particle incorporation on the pore structure and filtration characteristics of sintered stainless steel filters. By systematically varying the flake particle content under fixed compaction and sintering conditions, the relationship between pore geometry, particle capture behavior, and pressure drop is examined. This work aims to establish pore-structure-driven design principles for achieving high filtration efficiency while minimizing permeability loss, thereby providing a rational framework for the development of high-performance metal gas filters for semiconductor applications.

2. Experimental

Fine flake-shaped powders were prepared from commercial SS316L powders (PF-13F, Epson Atmix, Japan) using a planetary ball mill with zirconia (ZrO_2) vials and 1 mm ZrO_2 balls. Stearic acid (1 wt.%) and ethanol were used as a process control agent and a milling medium, respectively, and the ball-to-powder ratio was fixed at 10:1.

Sintered metal filters were fabricated using commercial irregular SS316L powders (Daido, Japan) as the matrix material. The base powder and the organic binder (M1, Atect, Japan) were mixed at a weight ratio of 100:3. To ensure uniform dispersion, the organic binder was melted and dispersed into the matrix powder at 130°C. Subsequently, fine flake-shaped powders were incorporated at 0.5, 1, 2, and 5 wt.%. To effectively prevent the agglomeration of the high-aspect-ratio flakes, the combined powders were first manually mixed using a mortar, followed by final homogenization using a vortex mixer. After homogenization, the powders were uniaxially compacted at 100 MPa for 1 min. Debinding was carried out under an argon atmosphere at 500°C with a heating rate of 1°C min^{-1}, and sintering was conducted under vacuum at 900°C for 1 h with a heating rate of 5°C min^{-1}.

Powder and filter microstructures were characterized by field-emission scanning electron microscopy (FE-SEM, JSM-6700F, JEOL, Japan), and the flake morphology was further examined by transmission electron microscopy (TEM, JEM-2010, JEOL, Japan). Particle size distributions were measured by dynamic light scattering (DLS, Beckman Coulter LS 13 320, USA). Pore size distribution and open porosity were evaluated by mercury intrusion porosimetry (MIP, AutoPore 9520, Micromeritics, USA), and gas permeability was measured using a capillary flow porometer.

Filtration performance was evaluated in accordance with the SEMI E70-0302 standard. The number of particles upstream and downstream of the filter was measured using a water-based condensation particle counter (Model 3789, TSI, USA), and the filtration efficiency was quantified in terms of the log reduction value (LRV). The pressure drop across the filter was measured by installing the filter between two digital pressure gauges. The inlet gas pressure was regulated using a pressure regulator, while the gas flow rate was controlled by a mass flow controller (MFC) positioned downstream of the filter. The pressure difference across the filter was recorded under steady-state conditions at a fixed pressure and flow rate.

3. Results and discussion

Fig. 1 shows the morphology and particle size characteristics of the powders used in this study. The irregular SS316L matrix powder (Fig. 1(a)) exhibits a rough, angular morphology with particle sizes in the tens of micrometers, whereas the pristine powder used for flake fabrication shows a spherical morphology with a narrower size distribution (Fig. 1(b)). The corresponding DLS results (Fig. 1(c)) confirm the smaller and more uniform size of the pristine powder. After 12 h of planetary ball milling, the powder undergoes a clear morphological transformation into fine flake-shaped particles (Fig. 1(d)). TEM analysis (Fig. 1(e)) confirms the formation of thin, high-aspect-ratio flakes at the submicrometer scale. The DLS result after milling (Fig. 1(f)) shows a pronounced reduction in characteristic particle size, indicating effective particle flattening and fragmentation during high-energy milling.

Fig. 2 shows the cross-sectional microstructures of sintered metal filters fabricated with different contents of fine flake-shaped powders. The reference filter without flake addition (Fig. 2(a)) exhibits relatively simple interparticle voids formed between irregular matrix powders. With increasing flake content (0.5-1 wt.%, Fig. 2(b-c)), thin flake-shaped particles are progressively introduced into the interstitial spaces between matrix particles, subdividing large pores into smaller and more irregular voids. This results in a more complex pore structure without apparent pore collapse. At higher flake contents (2-5 wt.%, Fig. 2(d-e)), excessive accumulation of flake particles leads to pronounced pore constriction and partial blockage, producing a highly fragmented pore network. These observations indicate that controlled flake addition effectively increases pore-structure complexity, while excessive incorporation results in over-modification of the pore network.

Fig. 3 presents the quantitative evolution of pore architecture and the resulting gas transport behavior of the sintered metal filters as a function of fine flake-shaped powder content. The pore size distribution and open porosity of the filters were evaluated using mercury intrusion porosimetry. The cumulative mercury intrusion curves (Fig. 3(a)) show comparable total intrusion volumes for all samples. This observation indicates that the fundamental volumetric porosity is largely preserved, consistent with the relative density remaining nearly constant at approximately 54-55% across all compositions.

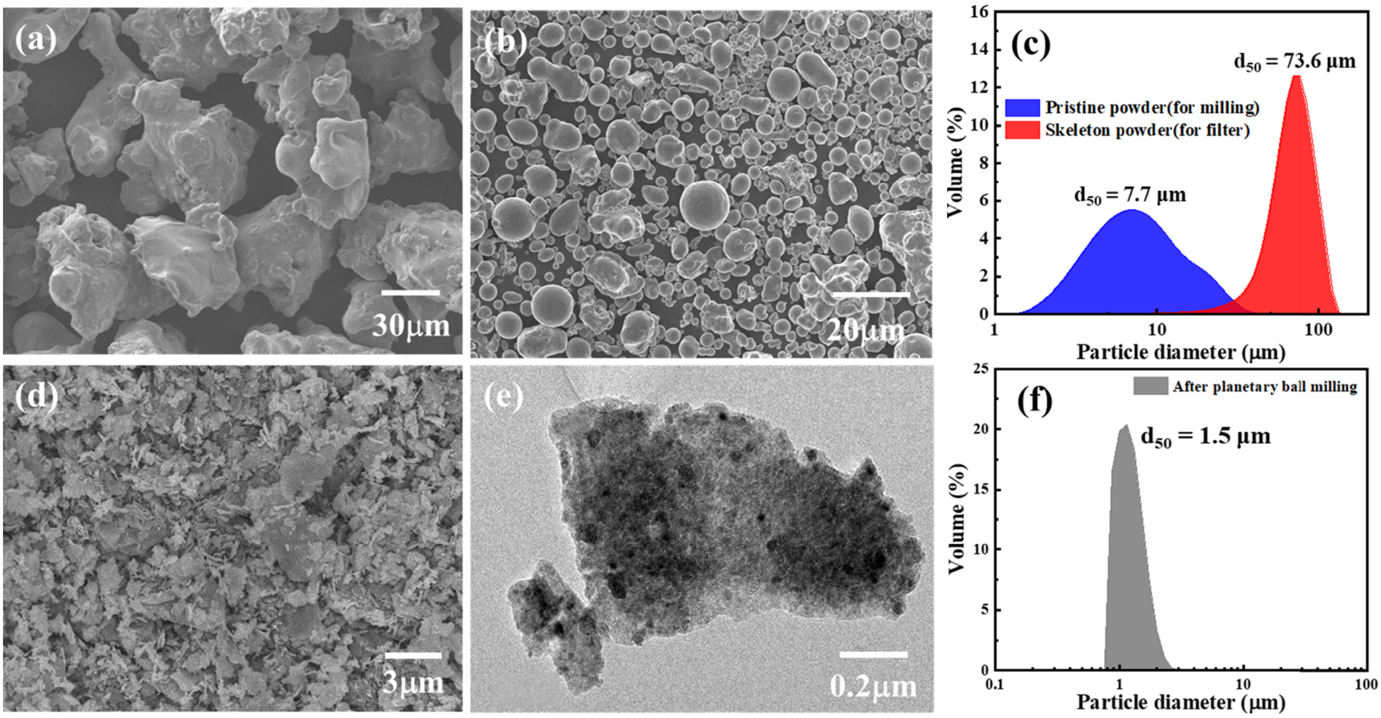

Fig. 1. Morphology and particle size characteristics of SS316L powders: (a) irregular matrix powder, (b) pristine spherical powder used for flake fabrication, (c) corresponding DLS particle size distributions, (d) SEM image of flake-shaped powder after 12 h of planetary milling, (e) TEM image showing thin flake-shaped morphology at the submicrometer scale, and (f) DLS particle size distribution of the milled flake powder

However, a detailed analysis of the structural connectivity reveals a critical transition. At low flake contents (≤1 wt.%), the open porosity remains robust and highly interconnected, measuring 39.2% at 0.5 wt.% and slightly increasing to 39.8% at 1 wt.%. This suggests that a controlled addition of flakes successfully integrates into the matrix without obstructing primary percolating pathways. Conversely, at higher flake contents, the open porosity progressively declines to 38.9% at 2 wt.% and more noticeably to 36.3% at 5 wt.%, accompanied by a corresponding increase in closed porosity from ~6% to 9.8%. This trend suggests that

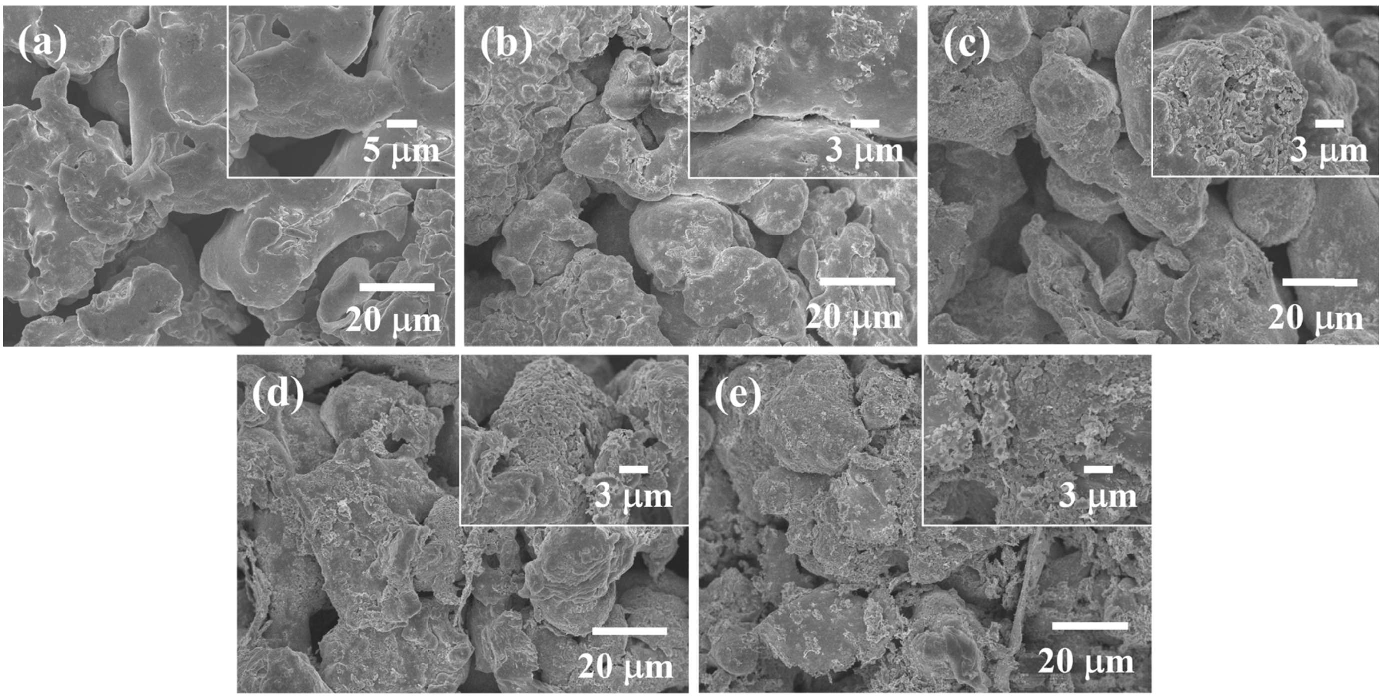

Fig. 2. Cross-sectional FE-SEM images of sintered metal filters fabricated with different contents of fine flake-shaped powders. The high-magnification FE-SEM images of the pore structures have been embedded as insets within their corresponding low-magnification counterparts: (a) 0 wt.%, (b) 0.5 wt.%, (c) 1 wt.%, (d) 2 wt.%, and (e) 5 wt.%

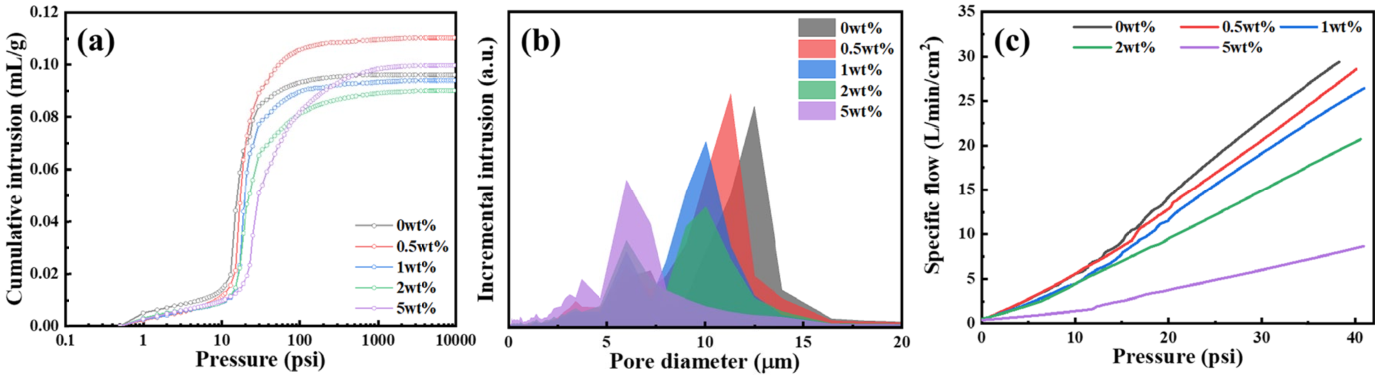

Fig. 3. (a) Cumulative mercury intrusion curves, (b) pore size distributions, and (c) gas permeability of sintered filters with varying fine flake-shaped powder contents

excessive flake incorporation promotes partial pore isolation and local pore closure, isolating previously continuous channels.

The pore size distributions shown in Fig. 3(b) reveal a systematic reduction in average pore diameter with increasing flake content. The average pore diameter decreases from 10.1 μm at 0.5 wt.% to 9.35 μm at 1 wt.%, followed by further reductions to 8.79 μm and 6.18 μm at 2 wt.% and 5 wt.%, respectively. This monotonic decrease confirms that flake-shaped powders effectively subdivide the interparticle voids between matrix powders, leading to selective pore size refinement. Fig. 3(c) shows the gas permeability of the filters. The permeability decreases with increasing flake content, reflecting the combined effects of reduced pore size, increased pore-structure complexity, and the gradual increase in closed porosity. Notably, at low flake contents (≤1 wt.%), a significant reduction in pore size is achieved while maintaining high open porosity and moderate permeability loss, whereas higher flake contents result in a pronounced deterioration in gas transport due to excessive pore constriction.

Fig. 4(a) shows the pressure drop measured at a constant inlet pressure of 4 bar. The pressure drop increases monotonically with increasing fine flake-shaped powder content, reflecting the combined effects of reduced pore size and increased pore-structure complexity. This trend is consistent with the permeability reduction observed in Fig. 3 and indicates progressively higher flow resistance as flake content increases. Fig. 4(b) presents the filtration efficiency evaluated according to the SEMI E70-0302 standard. In this study, the average number of particles passing through the filter per second was measured via particle counting analysis. Based on these measurements, the filtration performance was quantified using the log reduction value (LRV), which is defined by the following equation: LRV = log (N_i / N_o), representing the average number of particles per second entering (N_i) and exiting (N_o) the filter. As N_o decreases, the filtration efficiency improves, leading to a corresponding increase in the LRV. To ensure the statistical reliability and reproducibility of the results, the filtration efficiency for each sample was evaluated through three independent experimental trials [14].

The reference filter without flake addition exhibits an LRV of 4.22. With increasing flake content, the LRV increases to 4.32 at 0.5 wt.% and further to 4.50 at 1 wt.%, indicating a gradual improvement in particle capture efficiency. A more pronounced increase in LRV is observed at 2 wt.%, reaching a value of 5.35, corresponding to a substantial reduction in downstream particle concentration. However, this is also the point where the pore network undergoes detrimental over-modification. As the flake content exceeds 1 wt.%, the open porosity begins to decrease (to 38.9% at 2 wt.%) while closed porosity notably increases, leading to partial pore isolation. Consequently, although filtra-

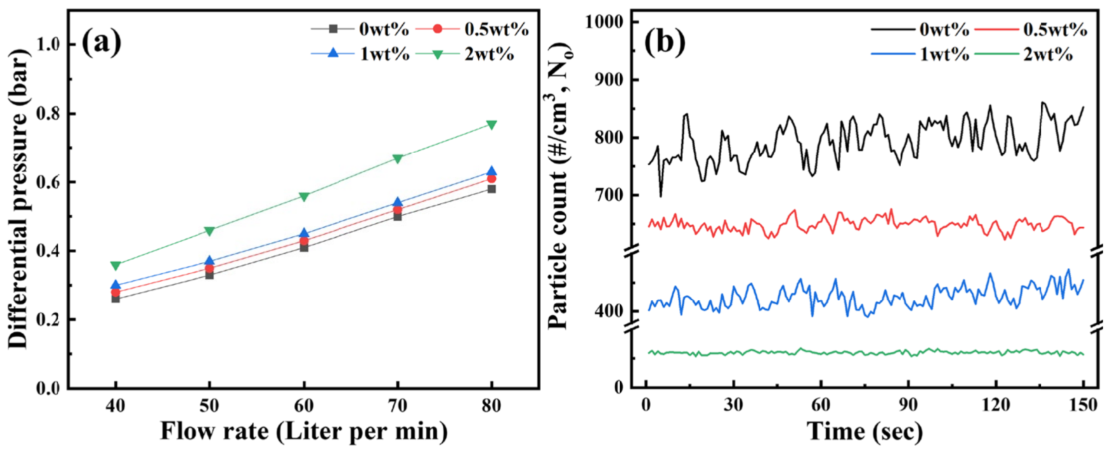

Fig. 4. (a) Pressure drop measured at an inlet pressure of 4 bar and (b) filtration efficiency expressed as log reduction value (LRV) for sintered filters with varying fine flake-shaped powder contents

tion efficiency improves with increasing flake content, this enhancement is accompanied by a disproportionate increase in pressure drop at higher flake contents. In particular, beyond the 1 wt.% critical threshold, the incremental gain in LRV becomes less favorable relative to the rapid increase in flow resistance. These results highlight the inherent trade-off between filtration efficiency and pressure drop arising from pore-structure modification via flake incorporation.

4. Conclusion

In this study, pore structure modification of sintered SS316L gas filters was achieved by incorporating fine flake-shaped powders into a conventional powder metallurgy process. The introduction of flake particles selectively reduced the average pore size by subdividing interparticle voids while largely preserving open porosity at low addition levels. Among the investigated compositions, the filter containing 1 wt.% flake-shaped powder exhibited the most favorable balance between filtration efficiency and pressure drop, showing a clear improvement in particle removal performance without a pronounced increase in flow resistance. In contrast, higher flake contents led to excessive pore constriction and increased closed porosity, resulting in a significant pressure drop. These results demonstrate that controlled incorporation of fine flake-shaped powders, particularly at low addition levels, provides an effective approach for tuning pore structure and enhancing filtration performance in sintered metal gas filters for high-purity gas applications.

Acknowledgments

This work was supported by the Technology Innovation Program (RS-2024-00431424, Development of Ni-Cr-Mo based components and field application technology for semiconductor manufacturing process gas control with surface roughness <Ra 0.125 um and RS-2025-16067075, Development of wet surface treatment technology for high strength metal-resin bonding in electric vehicle heater components) funded By the Ministry of Trade, Industry and Resources (MOTIR, Korea)

REFERENCES

[1] N.G. Orji, M. Badaroglu, B.M. Barnes, C. Beitia, B.D. Bunday, U. Celano, R.J. Kline, M. Neisser, Y. Obeng, A.E. Vladar, Nat. Electron. **1**, 532 (2018).
[2] Y. Lee, H.S. Kim, J.H. Lee, J. Semiconductor Tech. Sci. **22**, 145 (2022).
[3] V.M. Donnelly, A. Kornblit, J. Vac. Sci. Technol. A **31**, 050825 (2013).
[4] S.M. George, Chem. Rev. **110**, 111 (2010).
[5] M.S.A. Heikkinen, N.H. Harley, J. Aerosol Sci. **31**, 721 (2000).
[6] H. Singh, P. Saxena, Y.M. Puri, CIRP J. Manuf. Sci. Technol. **33**, 339 (2021).
[7] J.H. Zhao, Z.L. Xie, T. Zhong, T. Sun, K. Fezzaa, Y. Cai, J.Y. Huang, S.N. Luo, Mater. Sci. Eng. A **821**, 141593 (2021).
[8] M. Kim, M.-J. Lee, S.-J. Yun, P.-Y. Kim, H. J. Kim, J. Kim, J.W. Lee, J.-Y. Yun, J. Powder Mater. **32**, 299 (2025).
[9] K. Essa, P. Jamshidi, J. Zou, M.M. Attallah, H. Hassanin, Mater. Des. **138**, 21 (2018).
[10] S.A. Hosseini, H.V. Tafreshi, Sep. Purif. Technol. **74**, 160 (2010).
[11] X. Kong, Z. Li, D. Cai, B. Shen, Y. Zhang, Chem. Eng. Sci. **202**, 282 (2019).
[12] D.H. Lee, S. Han, M.-H. Park, J.-Y. Yun, M. Ji, Y.-I. Lee, Powder Metall. **66**, 679 (2023).
[13] Y. Kim, J.Y. Kim, M. Son, W. Kwon, E.S. Lee, S.-T. Oh, J. Powder Mater. **32**, 383 (2025).
[14] M.-J. Lee, H.-J. Kim, D.-H. Kang, J. W. Lee, J.-Y. Yun, Metals. **14**, 665 (2024).